



Cite this: *CrystEngComm*, 2017, 19, 2187

## 3D hierarchical golden wattle-like TiO<sub>2</sub> microspheres: polar acetone-based solvothermal synthesis and enhanced water purification performance†

Xiang Sun, Shiping Xu, \* Yuan Gao, Min Yue, Qinyan Yue and Baoyu Gao 

3D hierarchical TiO<sub>2</sub> microsphere structures self-assembled from 1D nanostructures have attracted considerable research attention due to their unique microstructures and properties, and non-polar solvent-based solvothermal methods have been proved to be effective techniques to synthesize such structures. However, to the best of our knowledge, no successful products have been reported based on polar solvents in the available literature. Herein, for the first time, uniform and sophisticated golden wattle (*Acacia pycnantha*)-like TiO<sub>2</sub> microsphere structures, self-assembled from highly crystallized and radially grown 1D rutile nanorods, were successfully synthesized via a template-free solvothermal reaction using only polar acetone as the solvent in the presence of hydrochloric acid (HCl). The obtained samples showed good water purification performance, even superior to Degussa P25, owing to their unique 1D nanorod building block structure, fast electron transfer rate, excellent light harvesting capability and good crystallinity. In addition, a three-step growth mechanism of the golden wattle-like TiO<sub>2</sub> microspheres was proposed based on a time-dependent morphology and crystal form evolution process. The synthetic strategy for the golden wattle-like TiO<sub>2</sub> microspheres employed in this study provides new insights into the design of 3D hierarchical TiO<sub>2</sub> structures for practical environmental purification applications.

Received 12th January 2017,  
Accepted 21st March 2017

DOI: 10.1039/c7ce00080d

rsc.li/crystengcomm

Nowadays, the global scarcity of clean water and serious water pollution, especially that induced by refractory organics, threaten life and even the existence of animals and human beings. Photocatalysis, which can decompose almost all organic pollutants into carbon dioxide and water under mild conditions without producing secondary pollution, has attracted considerable research attention around the world in recent years.<sup>1–3</sup> The semiconductor material TiO<sub>2</sub> is considered to be the most promising photocatalyst for pollutant removal due to its high photocatalytic activity, non-toxicity, photostability, low-cost and environment-friendly features,<sup>4–7</sup> and has been widely studied in lithium-ion batteries (LIBs), dye-sensitized solar cells (DSSCs), and gas sensors *etc.*<sup>5,8–11</sup>

However, the wide application of TiO<sub>2</sub> in practical water purification is seriously limited by (1) the fast recombination of photo-generated electrons and holes,<sup>12</sup> (2) its low light utilization efficiency,<sup>13,14</sup> and (3) the inevitable agglomeration of the nano-sized photocatalyst in solution and the difficulty in sepa-

rating the photocatalyst from the liquid phase.<sup>5</sup> Many modifications of TiO<sub>2</sub> have been attempted to tackle the above problems and positive results have been achieved, such as noble metal loading to accelerate the photo-generated electron transfer rate,<sup>15</sup> non-metal element doping to extend the light response range of TiO<sub>2</sub>,<sup>15–18</sup> and TiO<sub>2</sub> fixation to prevent agglomeration and ease the recovery of nano-sized TiO<sub>2</sub>.<sup>19,20</sup> However, most of the above approaches address only one or a maximum of two of the three drawbacks of TiO<sub>2</sub>, and no method has been reported that can resolve all three problems in one stroke.

Recently, micron-sized 3D hierarchical TiO<sub>2</sub> nanostructures self-assembled from 1D nanostructures have attracted the attention of many researchers and have been widely applied in DSSCs,<sup>21</sup> photocatalysis<sup>22,23</sup> and LIBs.<sup>24</sup> Rui *et al.* prepared TiO<sub>2</sub> microspheres assembled from single crystalline rutile TiO<sub>2</sub> nanorods for DSSCs and achieved a remarkable power conversion efficiency of 8.22%.<sup>25</sup> Nguyen-Phan *et al.* successfully synthesized a sea urchin-like Ru-doped TiO<sub>2</sub> hierarchical architecture composed of rutile TiO<sub>2</sub> nanorods and enhanced the photocatalytic H<sub>2</sub> production of TiO<sub>2</sub> under visible light irradiation.<sup>26</sup> All of the outstanding performances of 3D hierarchical TiO<sub>2</sub> structures can be ascribed to their special hierarchical structure,<sup>27</sup> where the 1D nanostructure building blocks can accelerate the electron transfer rate, resulting in reduced

Shandong Key Laboratory of Water Pollution Control and Resource Reuse, School of Environmental Science and Engineering, Shandong University, Jinan 250100, China. E-mail: shiping.xu@sdu.edu.cn; Fax: +86 531 88364513; Tel: +86 531 88361812

† Electronic supplementary information (ESI) available. See DOI: 10.1039/c7ce00080d

recombination of electron–hole pairs.<sup>28,29</sup> Meanwhile, the hierarchical structures enlarge the surface area and enhance the light harvesting capability of TiO<sub>2</sub>.<sup>30–32</sup> In addition, the dimensions of 3D hierarchical TiO<sub>2</sub> structures are at the micro-scale; therefore, this kind of TiO<sub>2</sub> is less likely to aggregate in solution, and is easier to separate from the liquid phase and recycle.<sup>4,33</sup> Therefore, from the viewpoints of high activity and easy recovery, 3D hierarchical TiO<sub>2</sub> has great potential for application in photocatalysis for practical water purification.

In the existing literature, the preparation of 3D hierarchical TiO<sub>2</sub> structures self-assembled from 1D nanostructures usually involves template materials and a hydrothermal method.<sup>30,34</sup> However, the samples obtained with use of template materials usually have irregular shapes and poor crystallinity without calcination,<sup>35</sup> and the hydrolysis rate of the titanium precursor in aqueous solution is very fast and difficult to control during the hydrothermal process.<sup>36,37</sup>

Recently, solvothermal methods using organic solvents instead of aqueous solutions have been proved to be an effective approach to synthesize 3D hierarchical TiO<sub>2</sub> self-assembled from 1D nanostructures. For instance, Zhou *et al.* successfully synthesized a 3D dandelion-like TiO<sub>2</sub> nanostructure composed of rutile nanorods *via* a single-step solvothermal reaction using non-polar solvents.<sup>38</sup> Gao *et al.* prepared flower-like TiO<sub>2</sub> microspheres composed of rutile nanorods *via* a solvothermal process based on benzene–water interfaces.<sup>39</sup> It has been reported that, using a solvothermal approach, the hydrolysis rate of the titanium precursor can be easily controlled<sup>33</sup> and the obtained samples possess regular shapes.<sup>38</sup> In addition, solvothermal approaches are much cheaper than hydrothermal methods employing template materials.<sup>33</sup> However, until now, to the best of our knowledge, most of the methods for the successful synthesis of 3D hierarchical TiO<sub>2</sub> structures self-assembled from 1D nanostructures have been based on non-polar solvents, and there have been no successful attempts to use only polar solvents.

In the available literature, acetone, a polar solvent, has been successfully employed to synthesize some TiO<sub>2</sub> sphere structures, although not 3D hierarchical TiO<sub>2</sub> microspheres self-assembled from 1D nanostructures, *via* a solvothermal method.<sup>35,40</sup> For example, Liu *et al.* synthesized smooth anatase TiO<sub>2</sub> sphere structures using only acetone as the solvent through a solvothermal approach.<sup>35</sup> Meanwhile, Gao *et al.* successfully prepared anatase TiO<sub>2</sub> mesoporous microspheres using an acetone–isopropanol mixture *via* a solvothermal method.<sup>40</sup> In addition, hydrochloric acid has been proved to be an effective morphology control agent for TiO<sub>2</sub>.<sup>21,41</sup> Therefore, although no successful 3D hierarchical TiO<sub>2</sub> structures self-assembled from 1D nanostructures have been reported from acetone-based solvothermal reactions, based on existing reports, it is reasonable to suppose that a solvothermal reaction employing polar acetone as the solvent in the presence of HCl would have great potential to produce sophisticated 3D ordered TiO<sub>2</sub> microsphere structures.

Herein, golden wattle (*Acacia pycnantha*)-like 3D hierarchical TiO<sub>2</sub> microsphere structures, self-assembled from 1D rutile

TiO<sub>2</sub> nanorods with radial growth from the center to the edge of the sphere, were successfully fabricated *via* a template-free solvothermal method using only acetone as the organic solvent and HCl as a morphology control reagent, and the growth mechanism was investigated as well. In addition, in this paper, the effect of HCl addition on the morphology and properties of the final products was investigated, and the photocatalytic activities of the synthesized samples were examined for phenol degradation, along with Degussa P25 for comparison.

## Experimental details

### 2.1 Synthesis

The golden wattle-like TiO<sub>2</sub> microspheres were synthesized *via* a solvothermal route with only acetone as the organic solvent. In a typical synthesis, acetone (20 ml), titanium *n*-butoxide (TBOT, 4 ml) and HCl (2 ml, 36 to 38 wt%) were mixed under vigorous stirring at ambient temperature. After stirring for 10 min, the mixture was transferred into a Teflon-lined autoclave with a capacity of 50 ml, and then the autoclave was tightly closed and kept at 150 °C for 8 h, followed by natural cooling to room temperature. Subsequently, the products were centrifuged and washed thoroughly with ethanol and deionized (DI) water several times, followed by drying at 80 °C for 12 h and calcination at 400 °C for 1 h to obtain the final product. The obtained sample was denoted as TiO<sub>2</sub>-2-8 in the text, where 2 stands for the volume of HCl addition (2 ml), and 8 represents the solvothermal reaction time (8 h). To investigate the effect of HCl addition on the properties of the final products, the volume of HCl was tuned from 0 ml to 6 ml, keeping all other experimental parameters and procedures unchanged, and the samples obtained were labelled as TiO<sub>2</sub>-X-8, where X is the volume of HCl added. Moreover, to understand the growth mechanism of the golden wattle-like TiO<sub>2</sub> microspheres, the solvothermal reaction time was adjusted from 0.5 h to 8 h, with HCl addition kept at 2 ml, and the samples obtained were named as TiO<sub>2</sub>-2-Y, where Y is the solvothermal reaction time. All reagents used in this work were of analytical grade and used without further purification.

### 2.2 Characterization

The phase and crystal structures of the obtained samples were characterized by X-ray diffraction (XRD) using a Bruker D8 Advance spectrometer with a scanning speed of 0.03° s<sup>-1</sup> over the 2θ range of 10° to 80° using Cu Kα radiation (λ = 1.5418 Å), and an operation voltage and current of 40 kV and 40 mA, respectively. The morphology of the samples was observed by field emission scanning electron microscopy (FESEM, JEOL JSM-6700F) and high resolution transmission electron microscopy (HRTEM, JEOL JEM-2100F). BET specific surface areas were determined from N<sub>2</sub> adsorption–desorption isotherms at 77 K recorded using an automated pore size and surface area analyzer (JW-BK122W, Beijing JWGB). The diffuse reflectance spectra (DRS) of the samples were measured using a UV-2550 UV-visible spectrophotometer (Shimadzu).

### 2.3 Photocatalytic activity test

The photocatalytic activity of the synthesized samples was tested for photocatalytic phenol degradation, along with Degussa P25 for comparison. The test was carried out in a cylindrical glass container exposed to air at room temperature and pressure with a light source located in the center of the container. The light source was a 14 W UV lamp (Shanghai JG Special Lighting) with the wavelength centered at 365 nm. In a typical photocatalytic reaction, a fixed mass of photocatalyst ( $\text{TiO}_2\text{-X-8}$  or P25, with a dosage of  $1.0 \text{ g L}^{-1}$ ) was dispersed in  $10 \text{ mg L}^{-1}$  phenol solution and stirred continuously. Before irradiation, the suspension was continuously agitated in the dark for 60 min to allow phenol to reach adsorption equilibrium on the surface of the photocatalyst. After the UV light was switched on, the samples were collected at the stated time intervals and subsequently filtered through a  $0.45 \mu\text{m}$  membrane filter to remove the photocatalyst, and the residual phenol concentration in the filtrate was determined using a UV-2450 UV-visible spectrophotometer (Shimadzu) at its maximum absorption wavelength at 270 nm.

## Results and discussion

Fig. 1 shows the morphology of the samples synthesized with different volumes of HCl addition. It can be clearly seen that HCl plays a very important role in controlling the morphology of the final products. Without HCl addition, for the  $\text{TiO}_2\text{-0-8}$  sample, uniform microspheres with smooth surfaces could be clearly observed in Fig. 1a and b, and the average diameter of the microspheres was around  $6.0 \mu\text{m}$ .

It is very interesting that with the introduction of 2 ml of HCl during the synthesis, the morphology of the obtained  $\text{TiO}_2\text{-2-8}$ , shown in Fig. 1c and d, differed from the smooth microspheres of  $\text{TiO}_2\text{-0-8}$  and appeared as golden wattle-like microsphere structures with diameters of around 2.5 to  $3.0 \mu\text{m}$ . It can be found that the golden wattle-like  $\text{TiO}_2\text{-2-8}$  microspheres were self-assembled through the radial growth of elongated crystalline nanorods, with widths and lengths of approximately 40–60 nm and 400–500 nm, respectively. Meanwhile, the 1D nanorod building blocks separated from each other from the core to the periphery of the spheres without obvious squeezing. The insets in Fig. 1c are high magnification images of the 1D nanorods of  $\text{TiO}_2\text{-2-8}$ , which clearly show that the nanorods can be depicted as a combination of quadrangular prism structures with half ellipsoid caps. To the best of our knowledge, this interesting structure of  $\text{TiO}_2\text{-2-8}$  has not been reported previously in the available literature, where only acetone was employed as the solvent. The growth mechanism of this structure will be systematically discussed later in this paper.

The architecture of the 1D nanorod building blocks of the  $\text{TiO}_2\text{-2-8}$  spheres was further investigated by HRTEM. The HRTEM image is shown in Fig. 1d, where two sets of lattice fringes perpendicular to each other with lattice spacings of 0.29 nm and 0.32 nm can be clearly observed, which can be ascribed to the interplanar spacing of the (001) and (110) planes

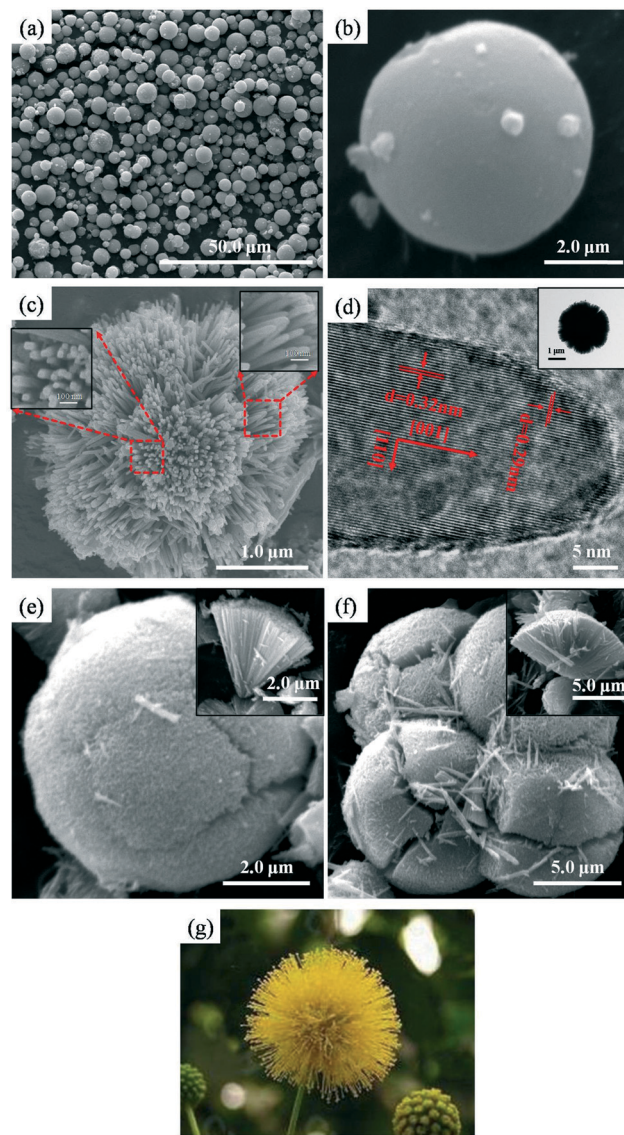


Fig. 1 Morphology of the samples synthesized with different volumes of HCl added: (a and b) FESEM images of  $\text{TiO}_2\text{-0-8}$ ; (c) FESEM image of  $\text{TiO}_2\text{-2-8}$ , inset: high magnification images of the 1D nanorods of  $\text{TiO}_2\text{-2-8}$ ; (d) HRTEM image of the 1D nanorods of  $\text{TiO}_2\text{-2-8}$ , inset: TEM image of a typical  $\text{TiO}_2\text{-2-8}$  sphere; (e and f) FESEM images of  $\text{TiO}_2\text{-4-8}$  and  $\text{TiO}_2\text{-6-8}$ , respectively, insets: sectional images of  $\text{TiO}_2\text{-4-8}$  and  $\text{TiO}_2\text{-6-8}$ , respectively; (g) image of an actual golden wattle with rods radially grown from the core to the edge.

of rutile  $\text{TiO}_2$ , respectively,<sup>21,31,41</sup> confirming the single-crystal nature of the rutile  $\text{TiO}_2$  nanorods in the  $\text{TiO}_2\text{-2-8}$  sample.

HRTEM observation of the  $\text{TiO}_2\text{-2-8}$  sample indicated that the  $\text{TiO}_2$  nanorod building blocks grew along the [001] direction,<sup>7,21,33,38</sup> parallel to the *c*-axis,<sup>33</sup> and the main exposed surfaces of the nanorods are {110} facets.<sup>34</sup> These results are consistent with previous research.<sup>7,21,32</sup> It has been reported that  $\text{Cl}^-$  can preferentially adsorb onto the (110) planes of rutile, and promote  $\text{TiO}_2$  nanorod growth along the [001] direction,<sup>42,43</sup> resulting in the formation of 1D rutile  $\text{TiO}_2$  nanorods in this study. Moreover, it is well known that the growth rate of crystals is related to the strength of chemical bonds.

According to the periodic bond chain (PBC) theory, the strongest chemical bonds usually lead to the fastest growth rate,<sup>44,45</sup> and the fastest growing plane tends to disappear in the end compared to the others.<sup>21</sup> Theoretical calculation shows that for a rutile lattice, the surface energy is  $E(110) < E(100) < E(101) < E(001)$ .<sup>21,46,47</sup> Therefore, consistent with the PBC theory, the  $\{001\}$  planes gradually disappeared at the periphery of the microspheres, and  $\{110\}$  facets were the main exposed planes of the nanorods, resulting in an interesting architecture of the 1D rutile nanorods consisting of a combination of quadrangular prisms with half ellipsoid caps, as observed in the FESEM images.

Different from the golden wattle-like microsphere structure of  $\text{TiO}_2$ -2-8, by further increasing the volume of HCl addition to 4 ml and 6 ml during synthesis, the morphologies of the as-prepared samples ( $\text{TiO}_2$ -4-8 and  $\text{TiO}_2$ -6-8) presented tennis ball-like microsphere structures consisting of densely packed crystalline nanorods, and the aspect ratios of the 1D nanorod building blocks increased sharply compared to the  $\text{TiO}_2$ -2-8 sample. In addition, the sizes of the  $\text{TiO}_2$ -4-8 and  $\text{TiO}_2$ -6-8 microspheres were around 7.5  $\mu\text{m}$  and 10  $\mu\text{m}$ , respectively, and were much larger than that of the  $\text{TiO}_2$ -2-8 sample.

The morphology variations induced by an increase in the volume of HCl added during the solvothermal process were accompanied by a downward trend in the BET specific surface areas of the samples, as shown in Table 1. This result is consistent with previous research, where the BET specific surface area of a series of 3D hierarchical rutile  $\text{TiO}_2$  architectures, synthesized *via* an acid-hydrothermal method, decreased with an increase in the HCl concentration employed during the synthesis.<sup>21</sup>

Besides the morphology, the crystallinity and UV-visible absorption spectra of the synthesized samples also varied considerably with an increase in the volume of HCl added during the synthesis process.

The XRD patterns shown in Fig. 2 indicate that the sample obtained without HCl addition ( $\text{TiO}_2$ -0-8) was pure anatase  $\text{TiO}_2$  (JCPDS No. 21-1272), which is consistent with the results reported by Liu *et al.*<sup>35</sup> However, with the addition of HCl, the diffraction peaks of the  $\text{TiO}_2$ -2-8,  $\text{TiO}_2$ -4-8 and  $\text{TiO}_2$ -6-8 samples could all be assigned to rutile phase  $\text{TiO}_2$  (JCPDS No. 21-1276) with good crystallinity, particularly in the (110) plane,<sup>25</sup> which is in good agreement with the HRTEM image shown in Fig. 1d. It has been reported that strongly acidic conditions and the presence of  $\text{Cl}^-$  ions in the solution are favourable for rutile formation,<sup>43</sup> and this was definitely reconfirmed in this study. In addition, it can also be found that the  $\text{TiO}_2$ -2-8 sample possessed the best crystallinity compared to the other three samples, as shown by it having the sharpest and strongest XRD diffraction peaks.

**Table 1** BET specific surface areas of the samples synthesized with different volumes of HCl added

Sample	$\text{TiO}_2$ -0-8	$\text{TiO}_2$ -2-8	$\text{TiO}_2$ -4-8	$\text{TiO}_2$ -6-8
BET specific surface area ( $\text{m}^2 \text{g}^{-1}$ )	134.6	42.8	34.6	30.9

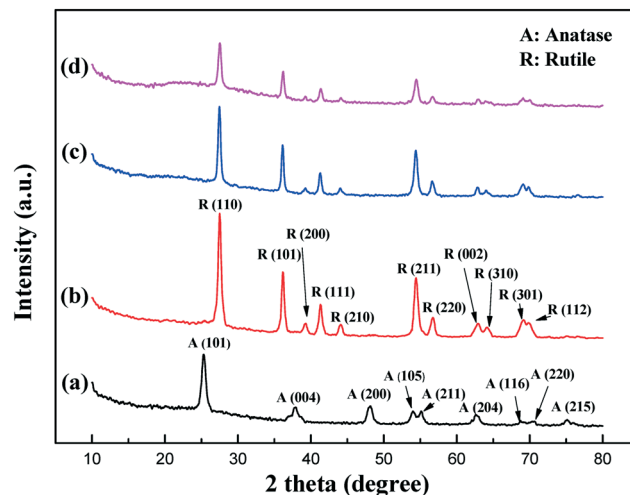


**Fig. 2** XRD patterns of the obtained samples prepared with different volumes of HCl added: (a)  $\text{TiO}_2$ -0-8, (b)  $\text{TiO}_2$ -2-8, (c)  $\text{TiO}_2$ -4-8, and (d)  $\text{TiO}_2$ -6-8.

Fig. 3 contains the UV-visible absorption spectra of all the prepared samples, and it can be seen that compared to  $\text{TiO}_2$ -0-8, the samples synthesized with HCl addition ( $\text{TiO}_2$ -2-8,  $\text{TiO}_2$ -4-8 and  $\text{TiO}_2$ -6-8) showed an obvious red shift of the absorption threshold. Combined with the XRD analysis, the variation of the absorption threshold of the samples can be ascribed to their different crystal phases: rutile *vs.* anatase. It is well known that the band gap of rutile  $\text{TiO}_2$  is 3.0 eV, which is narrower than the 3.2 eV band gap of anatase  $\text{TiO}_2$ ,<sup>9</sup> and the band gap values of the four synthesized samples ( $\text{TiO}_2$ -0-8: 3.2 eV,  $\text{TiO}_2$ -2-8/ $\text{TiO}_2$ -4-8/ $\text{TiO}_2$ -6-8: 3.0 eV) agreed well with their corresponding crystal form, calculated by employing the Kubelka–Munk function with the plot of  $(\alpha h\nu)^{1/2}$  versus  $h\nu$  shown in Fig. S1.† The red shift of the absorption threshold for the samples with HCl addition could result in more light absorption; from this point of view, it would enhance the light-induced photocatalytic activity of the obtained products.

Based on the above results and analyses, the function of HCl in the formation of  $\text{TiO}_2$  microspheres with various morphologies and properties is illustrated in Fig. 4. When there was no HCl addition, the obtained samples were smooth anatase microspheres, which agreed well with previous studies; Liu *et al.*<sup>35</sup> and Wang *et al.*<sup>48</sup> reported that acetone underwent aldol condensation in the presence of a titanium precursor, and the water molecules released during the condensation served as the oxygen source to generate  $\text{TiO}_2$  nanoparticles, which subsequently aggregated together to form anatase  $\text{TiO}_2$  microspheres because of van der Waals forces.<sup>35,48</sup>

Different from the smooth sphere structures obtained with no HCl addition, hierarchically golden wattle-like or tennis ball-like microspheres self-assembled from 1D rutile  $\text{TiO}_2$  nanorods were obtained when a certain amount of HCl was added. It has been reported that a low pH and the presence of  $\text{Cl}^-$  ions favour the formation of rutile  $\text{TiO}_2$ ,<sup>21,43</sup> and the selective adsorption of  $\text{Cl}^-$  ions on the rutile (110) plane promotes nanorods growth along the [001] direction;<sup>49</sup> moreover,

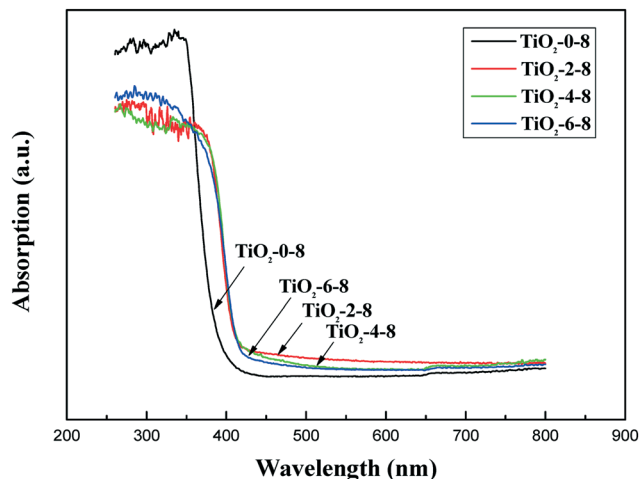


Fig. 3 UV-visible absorption spectra of the samples synthesized with different volumes of HCl added.

the presence of 4<sub>2</sub> screw axes along the crystallographic *c*-axis within rutile TiO<sub>2</sub> is also believed to be a guiding force for the formation of 1D rutile nanorods.<sup>38,50,51</sup> Therefore, 1D rutile TiO<sub>2</sub> nanorod building blocks were formed when HCl was present in the reaction solution during the solvothermal process, and the formed nanorods subsequently self-assembled together to form golden wattle-like or tennis ball-like microsphere structures to reduce the total free energy.<sup>38</sup>

It is worth noting that, depending on the amount of HCl addition, the self-assembly patterns of the 1D rutile nanorods were different. With a suitable amount of HCl addition, hierarchical golden wattle-like microsphere structures could be obtained; however, when too much HCl was added, the generated 1D nanorods were densely packed together to form tennis ball-like microspheres. It has been reported that less nanocrystalline nuclei are formed when the solution pH is lower;<sup>41,52</sup> therefore, a smaller number of microspheres would be generated when more HCl was present in the reaction solution, which was confirmed in this study by the in-

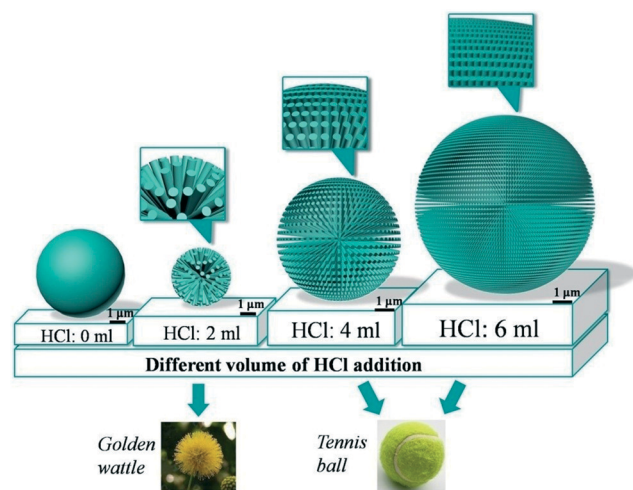


Fig. 4 Schematic illustration of the sphere structures synthesized with various amounts of HCl addition during the solvothermal reaction.

crease in the size of the produced microspheres when more HCl was added, as illustrated in Fig. 4. In addition, as observed from the FESEM images shown in Fig. 1e and f, the lower number and larger size of the produced microspheres resulted in the generation of 1D nanorods with a bigger aspect ratio and a higher surface energy. To obtain a stable product, different from the loosely packed golden wattle-like microspheres, the more slender nanorod building blocks generated with more HCl added had to pack together more tightly to form a tennis ball-like product to reduce the total free energy of the system.<sup>38</sup> Meanwhile, the dense packing of the 1D nanorod building blocks brought about a decline in many aspects of the final products, such as their BET specific surface area, light harvesting capability and carrier transportation properties. Therefore, the amount of HCl added during the solvothermal process is crucial for the properties of the final products, in terms of both their physical-chemical characteristics and their photocatalytic behaviour.

Phenol is appreciably soluble in water and toxic to living organisms. Furthermore it is very difficult to degrade. Therefore, in this paper, phenol was selected as the probe to evaluate the photocatalytic activity of the products synthesized with different amounts of HCl addition during the solvothermal reaction, along with Degussa P25 for comparison, and the results are shown in Fig. 5. It can be clearly seen that the photocatalytic activity of TiO<sub>2</sub>-2-8 was superior to that of the other samples synthesized with different volumes of HCl addition, and was even better than that of P25, which possesses great photocatalytic activity owing to its unique anatase-rutile mixed crystal phase,<sup>33</sup> excellent nanoscale dispersibility and relatively large specific surface area.

It is well accepted that the high photocatalytic activity of TiO<sub>2</sub> is related to its low electron-hole recombination rate, mature crystallinity and large specific surface area.<sup>53,54</sup> In this study, the relatively good photocatalytic performance of TiO<sub>2</sub>-2-8 can be attributed to the combined effects of the following factors: firstly, the loosely packed 1D nanorod building blocks could reduce the recombination of photo-generated electron-hole pairs, since it has been reported that 1D nanorods can offer pathways for electrons and accelerate their transportation,<sup>28,29</sup> and the smooth surfaces and high crystallinity of the 1D nanorods can suppress electron trapping at surface defects;<sup>55</sup> secondly, the golden wattle-like 3D hierarchical structure could enhance the light harvesting capability of TiO<sub>2</sub>-2-8 owing to the more efficient penetration, reflection and scattering of UV light within the whole 3D space of the microspheres;<sup>5,30</sup> thirdly, the larger BET specific surface area of TiO<sub>2</sub>-2-8 compared to TiO<sub>2</sub>-4-8 and TiO<sub>2</sub>-6-8 could provide more active adsorption sites, which is also beneficial for phenol degradation.<sup>8,56</sup>

In addition, the dimensions of the TiO<sub>2</sub>-2-8 sample were at the micron scale, so the sample was less likely to aggregate in solution and could be easily recovered by gravity sedimentation or membrane filtration without causing serious membrane fouling after pollutant removal. A set of detailed experiments to confirm this, along with a reusability study of TiO<sub>2</sub>-

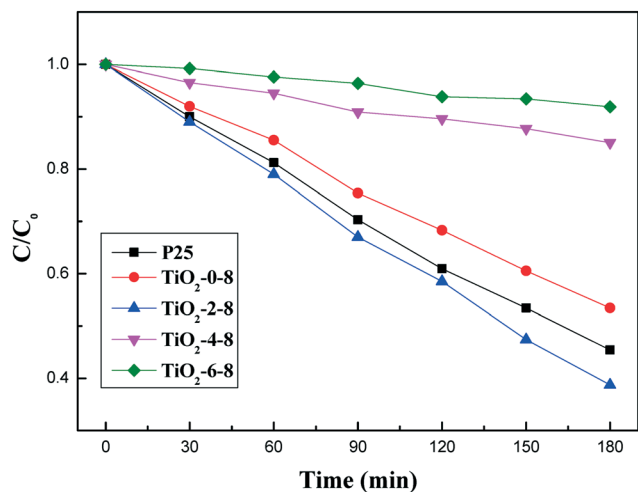


Fig. 5 Photocatalytic degradation of phenol by the different photocatalysts under UV light irradiation.

2-8, is currently being performed by our group, and will be reported later. Considering its good photocatalytic activity with the advantages of easy recovery and reusability, TiO<sub>2</sub>-2-8 possesses good potential for practical water purification.

In order to better understand the growth mechanism of the golden wattle-like TiO<sub>2</sub>-2-8 microspheres, which showed the best photocatalytic activity, time-dependent experiments were carried out, and the obtained products at different growth stages were investigated by FESEM and XRD, with the results shown in Fig. 6 and 7.

It can be clearly seen that at the early stage (0.5 h), particles with irregular shapes were dominant in the product, along with some short nanorods with small aspect ratios, designated by the red square shown in Fig. 6a. When the solvothermal reaction time increased to 1 h, for the TiO<sub>2</sub>-2-1 sample (Fig. 6b), distinct nanorod structures with lengths of around 500 nm could be readily observed, but they were still surrounded by many irregular particles. As the reaction time was extended to 2 h and 4 h, with the corresponding images shown in Fig. 6c and d, microsphere structures composed of 1D nanorod building blocks appeared, and became more mature, with fewer aggregated particles remaining on their surfaces. When the solvothermal reaction was prolonged to 8 h, no obvious particles and only golden wattle-like microsphere structures could be observed in the product. Therefore, it is reasonable to suppose that, during the 8 h solvothermal reaction, the morphology of the products in the system varies with time continuously, from irregularly aggregated particles to the final microsphere structures self-assembled from 1D nanorods.

From the XRD results of the time-dependent experiments shown in Fig. 7, it can be found that, in the early stages of the synthesis, when the solvothermal reaction time was less than 8 h, the crystallinities of the obtained samples were not mature, and both anatase and rutile TiO<sub>2</sub> could be found in their XRD patterns. With the extension of the solvothermal reaction time, finally to 8 h, the crystallinities of the products became more mature, and transformed from an anatase-rutile

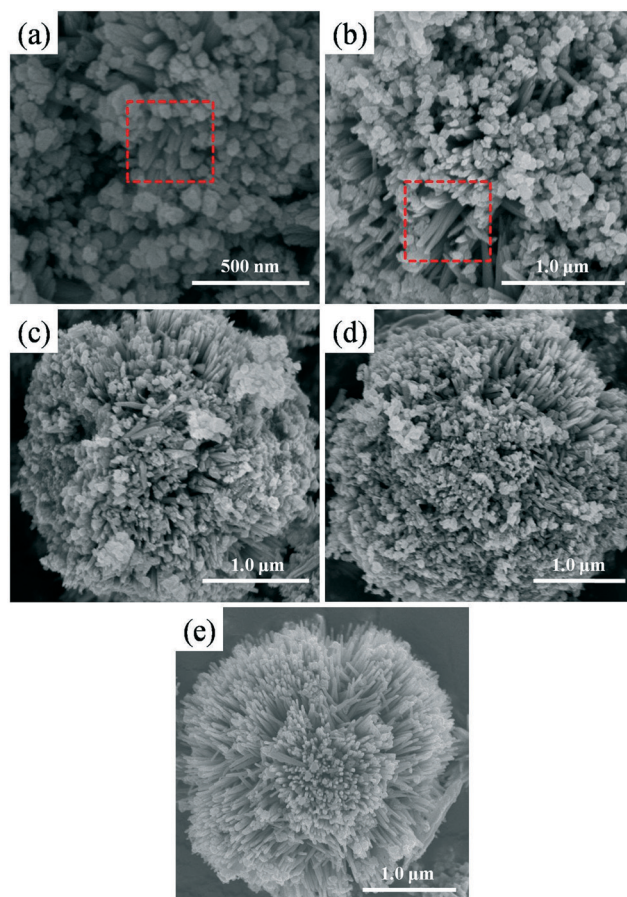


Fig. 6 FESEM images of the morphology evolution of TiO<sub>2</sub>-2-Y synthesized with different reaction times: (a) 0.5 h, (b) 1 h, (c) 2 h, (d) 4 h, and (e) 8 h.

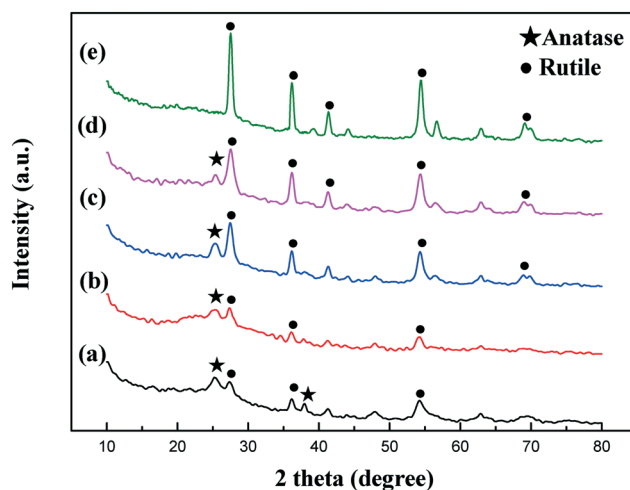


Fig. 7 XRD patterns of the crystal form evolution of TiO<sub>2</sub>-2-Y prepared with different reaction times: (a) 0.5 h, (b) 1 h, (c) 2 h, (d) 4 h, and (e) 8 h.

tile mixture to pure rutile TiO<sub>2</sub> in the TiO<sub>2</sub>-2-8 sample, along with the morphology changes.

It has been reported that, without HCl addition, acetone can react with a titanium precursor to form anatase TiO<sub>2</sub>

particles.<sup>35,48</sup> However, in this study, by combining FESEM observations with XRD analysis, it can be inferred that, during a prolonged solvothermal reaction, the TiO<sub>2</sub> particles composed of an anatase–rutile mixture that formed at the early stage of the reaction would dissolve and recrystallize to form pure rutile nanorods, owing to the strong acidic conditions and presence of Cl<sup>-</sup> ions.<sup>21,43</sup> Moreover, to reduce the free energy, the formed rutile nanorods further self-assembled together and finally formed the golden wattle-like sphere structures. Therefore, a possible mechanism for the generation of the golden wattle-like microspheres could be described as follows: (i) fast nucleation and nuclei growth; (ii) nanoparticle dissolution and recrystallization; (iii) nanorod growth and self-assembly.

## Conclusion

In summary, golden wattle-like 3D hierarchical TiO<sub>2</sub> microspheres self-assembled from radially grown 1D rutile nanorods were successfully synthesized *via* a template-free solvothermal method by using only polar acetone as the solvent and hydrochloric acid as a morphology control agent. The obtained golden wattle-like TiO<sub>2</sub> microspheres possessed superior phenol removal capability, even compared to Degussa P25, owing to their elaborate 3D hierarchical structure, unique 1D nanorod building blocks and excellent light harvesting capability. The growth mechanism of the golden wattle-like TiO<sub>2</sub> microspheres was supposed to be a three-step process: (i) fast nucleation and nuclei growth; (ii) nanoparticle dissolution and recrystallization; (iii) nanorod growth and self-assembly. In addition, the amount of HCl added during the solvothermal reaction played an important role in adjusting the morphology and properties of the final products, such as their crystal form, BET specific surface area and light harvesting capability. With no or an excess amount of HCl addition, smooth anatase microspheres or rutile tennis ball-like microsphere structures could be obtained instead of the golden wattle-like microsphere structures. Considering their good pollutant removal capability, in addition to their easy recovery and good reusability compared to other nanosized photocatalysts, the golden wattle-like 3D hierarchical TiO<sub>2</sub> microspheres possess great potential for practical water purification applications.

## Acknowledgements

This work was supported by the National Natural Science Foundation of China (21607095), the Research Foundation for the Outstanding Young and Middle-aged Scientists of Shandong Province of China (BS2014HZ005), China Postdoctoral Science Foundation (2013M540550, 2014T70643), and the Taishan Scholar Program (ts201511003).

## Notes and references

- 1 Y. Ohko, I. Ando, C. Niwa, T. Tatsuma, T. Yamamura, T. Nakashima, Y. Kubota and A. Fujishima, *Environ. Sci. Technol.*, 2001, **35**, 2365–2368.
- 2 K. Nakata and A. Fujishima, *J. Photochem. Photobiol., C*, 2012, **13**, 169–189.
- 3 T. Ochiai and A. Fujishima, *J. Photochem. Photobiol., C*, 2012, **13**, 247–262.
- 4 L. Mao, Y. Wang, Y. Zhong, J. Ning and Y. Hu, *J. Mater. Chem. A*, 2013, **1**, 8101–8104.
- 5 L. Xiang, X. Zhao, J. Yin and B. Fan, *J. Mater. Sci.*, 2011, **47**, 1436–1445.
- 6 Z. Liu, J. Liu, J. Liu, L. Wang, G. Zhang and X. Sun, *Phys. Chem. Chem. Phys.*, 2014, **16**, 8808–8811.
- 7 L. Yu, Z. Li, Y. Liu, F. Cheng and S. Sun, *J. Power Sources*, 2014, **270**, 42–52.
- 8 S. Tian, H. Yang, M. Cui, R. Shi, H. Zhao, X. Wang, X. Wang and L. Zhang, *Appl. Phys.*, 2010, **104**, 149–158.
- 9 M. Ye, D. Zheng, M. Wang, C. Chen, W. Liao, C. Lin and Z. Lin, *ACS Appl. Mater. Interfaces*, 2014, **6**, 2893–2901.
- 10 L.-L. Lai and J.-M. Wu, *Ceram. Int.*, 2015, **41**, 12317–12322.
- 11 Z. Fan, F. Meng, J. Gong, H. Li and A. Li, *Ceram. Int.*, 2016, **42**, 6282–6287.
- 12 L. Wang, Z. Nie, C. Cao, M. Ji, L. Zhou and X. Feng, *J. Mater. Chem. A*, 2015, **3**, 3710–3718.
- 13 J. H. Pan, G. Han, R. Zhou and X. S. Zhao, *Chem. Commun.*, 2011, **47**, 6942–6944.
- 14 I. Tamiolakis, I. T. Papadas, K. C. Spyridopoulos and G. S. Armatas, *RSC Adv.*, 2016, **6**, 54848–54855.
- 15 S. Sakthivel, M. V. Shankar, M. Palanichamy, B. Arabindoo, D. W. Bahnemann and V. Murugesan, *Water Res.*, 2004, **38**, 3001–3008.
- 16 F. Huang, Z. Fu, A. Yan, W. Wang, H. Wang, Y. Wang, J. Zhang, Y. Cheng and Q. Zhang, *Cryst. Growth Des.*, 2009, **9**, 4017–4022.
- 17 W.-S. Wang, D.-H. Wang, W.-G. Qu, L.-Q. Lu and A.-W. Xu, *J. Phys. Chem. C*, 2012, **116**, 19893–19901.
- 18 L. G. Devi and R. Kavitha, *Appl. Catal., B*, 2013, **140–141**, 559–587.
- 19 A. Maki, T. Ebara and J. Mizuguchi, *Mater. Trans.*, 2009, **50**, 2087–2091.
- 20 D. Yamaguchi, S. Suzuki and J. Mizuguchi, *J. Chem. Eng. Jpn.*, 2008, **41**, 929–932.
- 21 J. Lin, Y. U. Heo, A. Nattestad, Z. Sun, L. Wang, J. H. Kim and S. X. Dou, *Sci. Rep.*, 2014, **4**, 5769.
- 22 M. Ge, J. W. Li, L. Liu and Z. Zhou, *Ind. Eng. Chem. Res.*, 2011, **50**, 6681–6687.
- 23 D. Zhang, G. Li, F. Wang and J. C. Yu, *CrystEngComm*, 2010, **12**, 1759–1763.
- 24 L. Wang, Z. Nie, C. Cao, Y. Zhu and S. Khalid, *J. Mater. Chem. A*, 2015, **3**, 6402–6407.
- 25 Y. Rui, Y. Li, Q. Zhang and H. Wang, *Nanoscale*, 2013, **5**, 12574–12581.
- 26 T. D. Nguyen-Phan, S. Luo, D. Vovchok, J. Llorca, S. Sallis, S. Kattel, W. Xu, L. F. Piper, D. E. Polyansky, S. D. Senanayake, D. J. Stacchiola and J. A. Rodriguez, *Phys. Chem. Chem. Phys.*, 2016, **18**, 15972–15979.
- 27 X. Bai, B. Xie, N. Pan, X. Wang and H. Wang, *J. Solid State Chem.*, 2008, **181**, 450–456.
- 28 J.-Y. Liao, B.-X. Lei, D.-B. Kuang and C.-Y. Su, *Energy Environ. Sci.*, 2011, **4**, 4079–4085.

- 29 S. S. Mali, H. Kim, C. S. Shim, P. S. Patil, J. H. Kim and C. K. Hong, *Sci. Rep.*, 2013, **3**, 3004.
- 30 S. Xu, Y. Gao, X. Sun, M. Yue, Q. Yue and B. Gao, *RSC Adv.*, 2016, **6**, 101198–101207.
- 31 Z. Zheng, B. Huang, X. Qin, X. Zhang and Y. Dai, *Chemistry*, 2010, **16**, 11266–11270.
- 32 G. Tian, Y. Chen, W. Zhou, K. Pan, C. Tian, X.-R. Huang and H. Fu, *CrystEngComm*, 2011, **13**, 2994–3000.
- 33 J. Zhou, G. Zhao, G. Han and B. Song, *Ceram. Int.*, 2013, **39**, 8347–8354.
- 34 Z. Sun, J. H. Kim, Y. Zhao, F. Bijarbooneh, V. Malgras, Y. Lee, Y. M. Kang and S. X. Dou, *J. Am. Chem. Soc.*, 2011, **133**, 19314–19317.
- 35 B. Liu, L.-M. Liu, X.-F. Lang, H.-Y. Wang, X. W. Lou and E. S. Aydil, *Energy Environ. Sci.*, 2014, **7**, 2592–2597.
- 36 T. Tong, J. Zhang, B. Tian, F. Chen, D. He and M. Anpo, *J. Colloid Interface Sci.*, 2007, **315**, 382–388.
- 37 X. C. Jiang, T. Herricks and Y. N. Xia, *Adv. Mater.*, 2003, **15**, 1205–1209.
- 38 J. Zhou, G. Zhao, B. Song and G. Han, *CrystEngComm*, 2011, **13**, 2294–2302.
- 39 S. Yang and L. Gao, *Mater. Chem. Phys.*, 2006, **99**, 437–440.
- 40 L. Gao, X. Li, H. Hu, G. Li, H. Liu and Y. Yu, *Electrochim. Acta*, 2014, **120**, 231–239.
- 41 W. Zhou, X. Liu, J. Cui, D. Liu, J. Li, H. Jiang, J. Wang and H. Liu, *CrystEngComm*, 2011, **13**, 4557.
- 42 E. Hosono, S. Fujihara, K. Kakiuchi and H. Imai, *J. Am. Chem. Soc.*, 2004, **126**, 7790–7791.
- 43 K.-S. Park, K.-M. Min, Y.-H. Jin, S.-D. Seo, G.-H. Lee, H.-W. Shim and D.-W. Kim, *J. Mater. Chem.*, 2012, **22**, 15981–15986.
- 44 P. Hartman and W. G. Perdok, *Acta Crystallogr.*, 1955, **8**, 521–524.
- 45 P. Hartman and W. G. Perdok, *Acta Crystallogr.*, 1955, **8**, 525–529.
- 46 B. J. Morgan, D. O. Scanlon and G. W. Watson, *J. Mater. Chem.*, 2009, **19**, 5175–5178.
- 47 W. Guo, C. Xu, X. Wang, S. Wang, C. Pan, C. Lin and Z. L. Wang, *J. Am. Chem. Soc.*, 2012, **134**, 4437–4441.
- 48 H. Y. Wang, J. Chen, S. Hy, L. Yu, Z. Xu and B. Liu, *Nanoscale*, 2014, **6**, 14926–14931.
- 49 S. J. Kim, S. D. Park, Y. H. Jeong and S. Park, *J. Am. Ceram. Soc.*, 1999, **82**, 927–932.
- 50 D. Sarkar, C. K. Ghosh and K. K. Chattopadhyay, *CrystEngComm*, 2012, **14**, 2683–2690.
- 51 J. G. Li, T. Ishigaki and X. D. Sun, *J. Phys. Chem. C*, 2007, **111**, 4969–4976.
- 52 E. Hosono, S. Fujihara, H. Lmai, I. Honma, I. Masaki and H. Zhou, *ACS Nano*, 2007, **1**, 273–278.
- 53 C. Miranda, H. Mansilla, J. Yáñez, S. Obregón and G. Colón, *J. Photochem. Photobiol., A*, 2013, **253**, 16–21.
- 54 Z. Fan, F. Meng, M. Zhang, Z. Wu, Z. Sun and A. Li, *Appl. Surf. Sci.*, 2016, **360**, 298–305.
- 55 Z. He, J. Liu, J. Miao, B. Liu and T. T. Yang Tan, *J. Mater. Chem. C*, 2014, **2**, 1381–1385.
- 56 J. Zhou, B. Song, G. Zhao and G. Han, *Nanoscale Res. Lett.*, 2012, **7**, 2–10.